EVALUATION OF THE SUPERCONDUCTING LLRF SYSTEM AT cERL IN KEK

F. Qiu#, S. Michizono, T. Miura, H. Katagiri, D. Arakawa, T. Matsumoto, T. Miyajima, K. Tsuchiya,
KEK, Tsukuba, Ibaraki, 305-0801, Japan

Abstract

A low level RF (LLRF) design is being currently developed within the compact Energy Recover Linac (cERL) at KEK. One challenging task is to achieve the high amplitude and high phase stability required by the accelerating fields of up to 0.1% and 0.1°, respectively. To improve the performance of the LLRF system, a gain scanning experiment for determining the optimal controller gain was carried out on the cERL. Furthermore, as a substitute for the traditional PI controller, a more robust H_∞-based multiple input multiple output (MIMO) controller was realized. This controller requires more detailed system information (transfer function or state equation), which can be acquired by using modern system identification methods. In this paper, we describe the current status of these experiments on the cERL.

INTRODUCTION

The cERL project, a test accelerator for the future light source 5-GeV ERL, is on-going at KEK. On the cERL, a high RF stability of 0.1% (in amplitude) and 0.1° (in phase) is required. The requirements are even higher in ERL (0.01% for amplitude, 0.01° for phase) [1, 2]. To achieve such high field precisions, a digital LLRF system has been developed, and several advanced controlling approaches have been implemented. We have evaluated the performance of the LLRF system and determined the optimal controlling gains. Furthermore, we have identified the transfer function of the LLRF system using modern system identification methods. Finally, we designed an H_∞-based MIMO controller and implemented it in both the cERL and the STF at KEK.

LLRF SYSTEM

Figure 1 shows a schematic diagram of the LLRF system on the cERL. The main components include a digital board, resonant cavities, a clock distribution system, a tuner controlling system, a Klystron/IOT, and a fast interlock system.

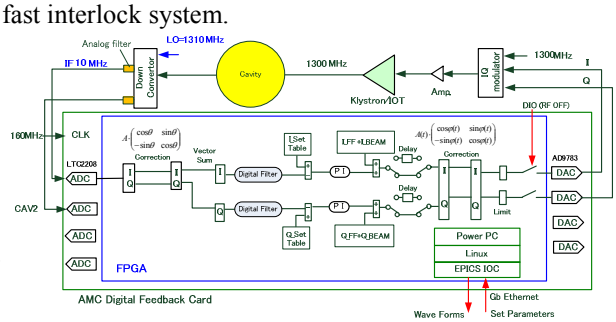

Figure 1: Schematic of LLRF system in cERL.

The 1.3 GHz RF signal from the IQ modulator is amplified by the Klystron and/or the IOT and is then fed into the cavity. The cavity-incident and pick-up signals are down-converted to 10 MHz IF signals. After being sampled at 160 MHz (the clock frequency) all of these signals are transmitted to the FPGA (Virtex-5 FXT) by a 16-bit ADC (LTC2208); each signal is processed inside the FPGA by digital signal processing (DSP) algorithms. The algorithms include the an IQ detector, an IIR filter, a PI feedback controller and a feed forward controller. The processed IQ signal is fed into the IQ modulator by a 16-bit DAC (AD9783) to re-generate the 1.3 GHz RF signal. Detailed information about the platform can be found in [3] and [4].

GAIN SCAN

To evaluate the system performance and determine the optimal controller gains of the LLRF system on the cERL, a test bench for the buncher cavity and injector cavity of the cERL is set up and a gain scanning experiment is carried out. The measured loaded Q value, Q_L, and the half-band width, $f_{1/2}$, of the different cavities are shown in Table 1[2].

Table 1: Cavity Parameters

Cavity	Q_L	$f_{1/2}$ [kHz]
Buncher	2.1e4	30.81
Inj1	1.2e6	0.54
Inj2	5.78e5	1.12
Inj3	4.8e5	1.35

A 1.3 GHz dummy cavity was selected as a replacement for the buncher cavity. For the injector cavities, an FPGA-based cavity simulator with an adjustable bandwidth is introduced. The performance of the LLRF system is evaluated for different proportional gains, K_P, and integral gains, K_I, (the definitions of these variables are presented in Fig. 2). The relationships between the real gains (K_P and K_I) and the FPGA input parameters (k_p and k_i) are $K_P = k_p/128$ and $K_I = k_i/262144$.

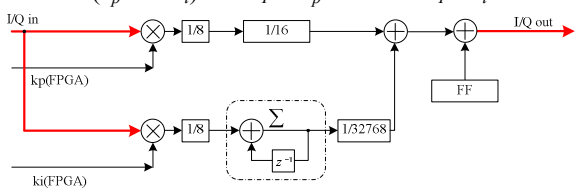

Figure 2: Schematic of the digital PI controller at cERL.

#qiufeng@post.kek.jp

Figures 3 and 4 show the system performance for different gains of either the dummy cavity or the buncher cavity, respectively. Here, "gains" refers to the real gains, K_P and K_I. It should be noted that for a better display of the 3D plot, as shown in Fig. 3, negative values are used for the stability data. The blue area in Fig. 3 corresponds to regions of poor performance gain, whereas the red area represents the desired gain (this color convention is reversed in the Fig. 4). It is clear that there is no significant difference between the optimal gains for the dummy and the buncher cavity. The optimal value of K_I is from 3e-4 to 4e-4, whereas the optimal K_P is between 0.59 and 0.66, according to Figs. 3 and 4, respectively. The field stabilities are 0.026% RMS for amplitude and 0.048° RMS for phase for the buncher cavity at the optimal gains.

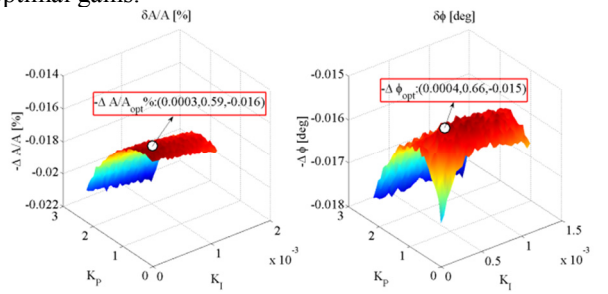

Figure 3: Gain scan result for the dummy cavity. The optimal gain is (3e-4, 5.9e-1) for the amplitude and (4e-4, 6.6e-1) for the phase (indicated by the white circle).

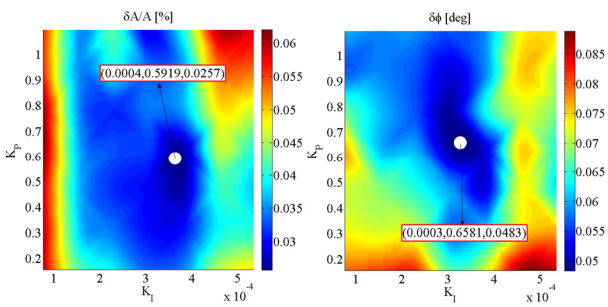

Figure 4: Gain scan result of the buncher cavity. The optimal gain is (4e-4, 5.9e-1) for the amplitude and (3e-4, 6.6e-1) for the phase (indicated by the white circle).

SYSTEM IDENTIFICATION

In more flexible control applications, such as H_∞-based MIMO control or iterative feed forward control, detailed knowledge (transfer function or state equation) about the controlled system is required. Modern system identification methods, however, provide an approach to acquiring detailed information about an un-known system. In this study, a black-box system identification model is selected, because this model does not require any prior information about the system.

To carry out the system identification experiment, the LLRF system should be operated in the pulse mode. The white noise signal should be added to the feed-forward signal during the flattop, as shown in Fig 5. It is strongly recommended that the white noise be injected into the IQ channel separately [5, 6], which means exciting only the I-channel and measuring the response in both I/Q output channels in the first step and then repeating the same process in the Q-channel in the second step. Further details regarding this approach can be found in [5].

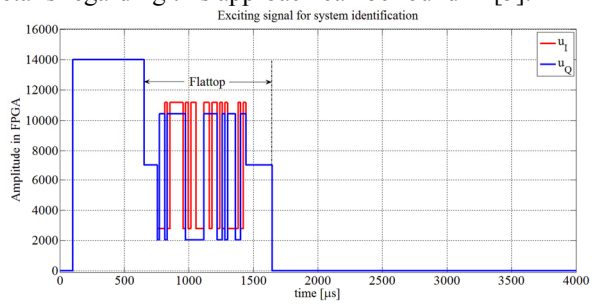

Figure 5: Input white noise signal during the flattop.

The system identification experiment was performed on both the cERL and the STF. Figure 6 shows the open-loop Bode plot of the identified transfer function including both of the on-diagonal and cross components of the STF LLRF system with 9-cell superconducting cavities. Fig. 7 compares the outputs of the identified 4th-order black box model and the measured outputs (located after the digital filter in Fig. 1) in the cERL LLRF system with a dummy cavity. Figure 7 shows that the identified model can accurately describe the behavior of the system.

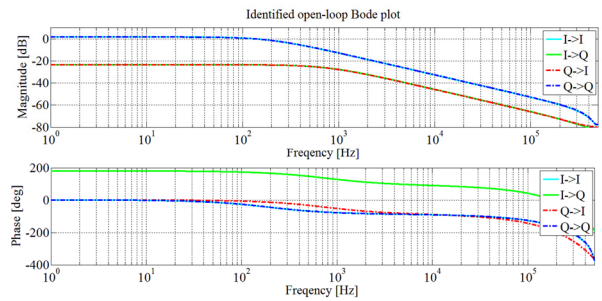

Figure 6: Identified open-loop Bode plot of the LLRF system on the STF with 9-cell superconducting cavities.

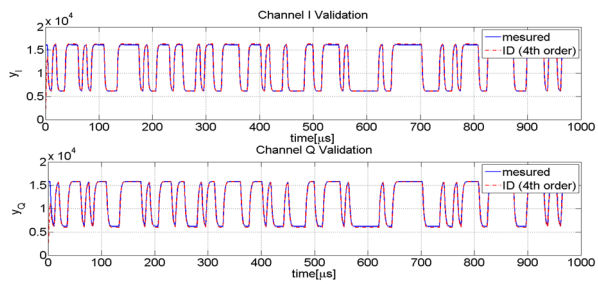

Figure 7: Comparison of the measured I/Q outputs (solid blue line) and the identified model I/Q outputs (dash-dot red line) in the cERL LLRF system with the dummy cavity.

MIMO CONTROLLER DESIGN

To improve the system performance, many well-known approaches such as the H_∞ method have been applied to

ISBN 978-3-95450-122-9

LLRF systems. The H_∞ method treats the controller design problem as a mathematical optimization problem. Relative to the traditional PI controller, H_∞-based MIMO controllers have advantages in a multivariable system with cross-coupling components.

To design an MIMO controller with the H_∞ method, knowledge about the open loop system is required; this could be realized by the system identification approach, as previously discussed. Usually the order of the designed controller developed by the traditional H_∞ method is too high to be implemented on an FPGA; however, [7] has provided a so-called HIFOO algorithm to obtain a fixed-order controller. The 2nd-order MIMO controller is selected on the basics of the result of [5]. The controller can be expressed by a 2 × 2 matrix shown in Eq. 1.

$$K(z)=\begin{pmatrix} K_{11}(z) & K_{12}(z) \\ K_{21}(z) & K_{22}(z) \end{pmatrix} \quad (1)$$

in which, the four elements are given by

$$K_{ij}(z)=\frac{k_{ij}+c_{ij}z^{-1}+d_{ij}z^{-2}}{1+a_{ij}z^{-1}+b_{ij}z^{-2}} \quad (2)$$

The controller is a kind of 2nd order IIR filter. The structure of the filter inside the FPGA is shown in Fig. 8.

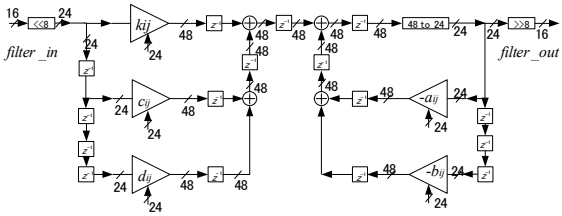

Figure 8: The main component of the MIMO controller. The register, the multiplier, the accumulator, and the bit widths are marked in detail.

This H_∞-based MIMO controller has been implemented on both the cERL and the STF. The results for the STF are presented in Fig. 9. The red stars indicate the field stability performance of the MIMO controller case; the blue diamonds correspond to the P controller case. Both the RMS stability (the deviation of the measured field from the reference trajectory of a single pulse) and the pulse-to-pulse stability (the deviation of the measured field from the reference trajectory from pulse to pulse) are considered here; detailed definitions of these two stability criteria can be found in [5].

As is shown in Fig. 9, the RMS stability of the MIMO controller case is not significantly better than that of the P controller case; however, in the case of the pulse-to-pulse stability, the phase performance was significantly improved. The main reason for this improvement is that in the MIMO controller there are cross-coupling components ($K_{12}(z)$ and $K_{21}(z)$ in Eq. 1) that might compensate for the coupling behaviors of the LLRF system; however, there are no coupling components in the P controller ($K_{12}(z) = K_{21}(z) = 0$). The pulse-to-pulse phase stability is 0.23° RMS for the P controller and 0.05° RMS for the MIMO controller (both without feed-forward controlling).

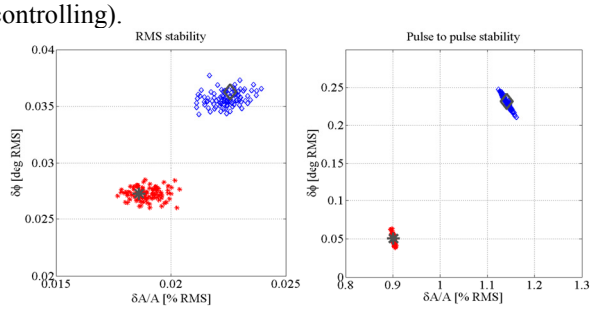

Figure 9: Left: The RMS stability of the MIMO controller (red stars) and P controller (blue diamonds). Right: The pulse-to-pulse stability of the MIMO controller (red stars) and P controller (blue diamonds).

SUMMARY

In this study, the performance of a digital LLRF system was evaluated on the cERL. The optimal proportional and integral gains are determined by using a gain scanning experiment. A closed-loop experiment with the buncher cavity shows that the measured field stabilities are 0.029% RMS for amplitude and 0.047° RMS for phase, which satisfy the cERL requirements, specifically (0.1% RMS for amplitude and 0.1° RMS for phase). Additionally, a system identification experiment was carried out on the cERL and the STF. Results show that the identified black box model can accurately describe the behavior of the system. Based on the identified model, an H_∞-based MIMO controller was designed and integrated with the LLRF system. According to the experimental results for the STF, the pulse-to-pulse phase stability of the MIMO controller was improved by 5 times relative to the traditional P controller.

REFERENCES

[1] T. Miyajima, "Beam Commissioning of Energy Recovery Linacs", IPAC'13, Shanghai, May 2013, FRXBB201.

[2] S. Sakanaka et al. "Progress in Construction of the 35-MeV Compact Energy Recovery Linac at KEK" IPAC'13, Shanghai, May 2013, WEPWA015.

[3] T. Miura et al. "Low-Level LLRF system for cERL", IPAC'10, Kyoto, May 2010, TUPEA048.

[4] S. Michizono et al., "Digital LLRF System for STF S1 Global", IPAC'10, Kyoto, May 2010, TUPEA047.

[5] C. Schmdt, "RF System Modeling and Controller Design for the European XFEL", Ph.D. thesis, Hamburg, 2010.

[6] C. Schmdt et al., "Parameter Estimation and Tuning of a Multivariable RF Controller with FPGA Technique for the Free Electron Laser FLASH", *American Control Conference*, Seattle, USA, 2008.

[7] J. V. Burke et al., "HIFOO A Matlab Package for Fixed-order Controller Design and H_∞ Optimization", *5th IFAC Symposium on Robust Control Design,* Toulouse, France, 2006.